Effect of Image Pair Temporal Gap on Spatiotemporal Fusion

Nahid Haghshenas [1], Ali Shamsoddini [2]*

[1] Dept. of RS and GIS, Tarbiat Modares University, Tehran, Iran - n.haghshenas@modares.ac.ir
[2] Dept. of RS and GIS, Tarbiat Modares University, Tehran, Iran - ali.shamsoddini@modares.ac.ir

KEY WORDS: Spatiotemporal Fusion Methods, MODIS, Landsat, Random Forest, ESTARFM, Temporal Gap.

ABSTRACT:

Despite significant advances in remote sensing and the growing availability of time-series data, challenges remain due to sensor limitations and the trade-off between spatial and temporal resolution. These constraints hinder the acquisition of datasets with both high spatial and temporal resolution. Spatiotemporal fusion (STF) algorithms have emerged as an effective solution, but the complexity of land surface processes can reduce their accuracy. Land surface temperature (LST) is a key parameter for agricultural monitoring, directly affecting crop growth, evapotranspiration, and plant stress detection. This study examines the impact of temporal intervals between input image pairs on STF accuracy using nine pairs of LST images from MODIS and Landsat sensors over agricultural lands, covering intervals of 32, 48, and 96 days. Two widely used STF algorithms, Random Forest (RF) and Enhanced Spatial and Temporal Adaptive Reflectance Fusion Model (ESTARFM), were applied for comparison. Results show a consistent decline in fusion accuracy with increasing temporal gaps. For RF, the Root Mean Square Error (RMSE) increased from 1.77 to 1.81 ˚K, while for ESTARFM, RMSE ranged from 1.69 to 2.63 ˚K. Similarly, the Peak Signal-to-Noise Ratio (PSNR) decreased from 23.20 to 21.17 in RF, and from 23.59 to 17.06 in ESTARFM. These findings highlight the importance of temporal interval as a critical factor in STF and reveal differing algorithm sensitivities to varying gaps. Overall, this study demonstrates the potential of LST-based spatiotemporal fusion for improving agricultural mapping and monitoring, emphasizing the need to consider temporal intervals when generating high-resolution temperature datasets over agricultural lands.

1. INTRODUCTION

Due to the limitations of individual satellite platforms or sensors, obtaining high-resolution data in both spatial and temporal dimensions remains challenging. For example, daily sensors such as MODIS provide LST data at low spatial resolution (1 km), while high spatial resolution sensors (100 meters or less) acquire data only at multi-day intervals due to limited coverage and orbital constraints (Guo et al., 2024). Furthermore, frequent cloud cover and haze make it difficult to obtain cloud-free images with both short temporal intervals and full spatial coverage (Zhu et al., 2021). Therefore, despite the increasing number of remote sensing satellites being launched, acquiring high-resolution data in both spatial and temporal dimensions remains challenging. Spatio-temporal data fusion (STF) offers an effective solution for generating high-resolution data in both domains. Various STF methods have been developed and can generally be categorized into four main groups: spatial weighting methods, spatial unmixing methods, hybrid methods, and learning-based methods (Wang et al., 2023). Weighting-based methods typically assume that pixels in low-resolution images are homogeneous and establish linear models between multi-temporal and multi-scale observations, using spatiotemporal weighting strategies to improve prediction accuracy. These methods, such as the Spatial and Temporal Adaptive Reflectance Fusion Model (STARFM) (Gao et al., 2006) and its enhanced version ESTARFM (Zhu et al., 2010), are flexible in applying different weighting functions to enhance fusion accuracy. Spatial unmixing-based methods assume that each low-resolution pixel is a linear combination of the spectral reflectance from various land cover classes found in a higher-resolution area. (Zhukov et al., 1999; Zurita-Milla et al., 2009; Zhu et al., 2016). Learning-based methods, on the other hand, model the nonlinear relationships between images of different resolutions (Chen et al., 2022). These include approaches such as dictionary-pair learning-based methods (Huang, Song, 2012) and artificial neural networks (Moosavi et al., 2015). Hybrid methods aim to integrate the strengths of various techniques to achieve better performance than any individual approach (Xiao et al., 2023).

In recent years, machine learning-based STF methods have gained popularity due to their remarkable ability to capture complex nonlinear patterns and deliver high accuracy. However, due to the dynamic nature of land surface features and the spatial-temporal complexities across different regions, the performance of these algorithms may vary under different conditions. Although a wide range of STF models has been developed over the past two decades, many of them have not yet been widely applied in real-world land monitoring. Therefore, in addition to theoretical improvements, extending their practical applications is essential for advancing STF technology

* Corresponding author

(Xiao et al., 2023). A significant reason for this limited practical use may be the lack of appropriate datasets (Xiao et al., 2023). Thus, the quality of input data plays a key role in the final results. While previous studies often used high-quality datasets with short temporal intervals between image pairs, such conditions are not always feasible, especially in regions where cloud-free images are difficult to obtain. Since the temporal gap between base image pairs varies across regions and times depending on image availability, it can significantly influence the performance of STF algorithms. In this study, the impact of different time intervals between image pairs on the spatiotemporal fusion of land surface temperature (LST) data was examined. The aim is to provide a more realistic understanding of STF algorithm performance under actual conditions. For evaluation, the widely adopted Random Forest algorithm, one of the most common machine learning methods, along with ESTARFM as a classic weighting-based model, were utilized. The structure of this paper is as follows: Section 2 introduces the data and study area; Section 3 describes the algorithms and evaluation metrics; Section 4 presents the results and discussion; and finally, Section 5 offers the conclusion of this paper.

2. STUDY AREA AND DATA

2.1 Study area

As shown in Figure 1, the study area is located in Yanco, within the Murrumbidgee River catchment in southeastern Australia, covering an area of approximately 40 × 80 km^2. The land use in this region is primarily irrigated cropland and pasture. Geographically, the area extends from -34.185° to -34.980° South latitude and from 145.834° to 146.769° East longitude. The topography is predominantly flat, with elevations ranging from 117 to 150 meters above sea level and minimal slope (Senanayake et al., 2021; Ye et al., 2020; Young et al., 2008). Yee et al., 2016).

Date of acquisition	Data Collection	Seasons	Time Interval (Day)
Jan 2, 2021	Landsat 8 LST product MOD11A	Summer	
Feb 2, 2021	Landsat 8 LST product MOD11A	Autumn	48
Mar 6, 2021	Landsat 8 LST product MOD11A	Autumn	
Jan 12, 2022	Landsat 8 LST product MOD11A	Summer	
Jan 20, 2022	Landsat 8 LST product MOD11A	Summer	32
Feb 13, 2022	Landsat 8 LST product MOD11A	Summer	
Jan 15, 2023	Landsat 9 LST product MOD11A	Summer	
Jan 31, 2023	Landsat 9 LST product MOD11A	Autumn	96
Apr 21, 2023	Landsat 9 LST product MOD11A	Autumn	

Table 1. The used datasets

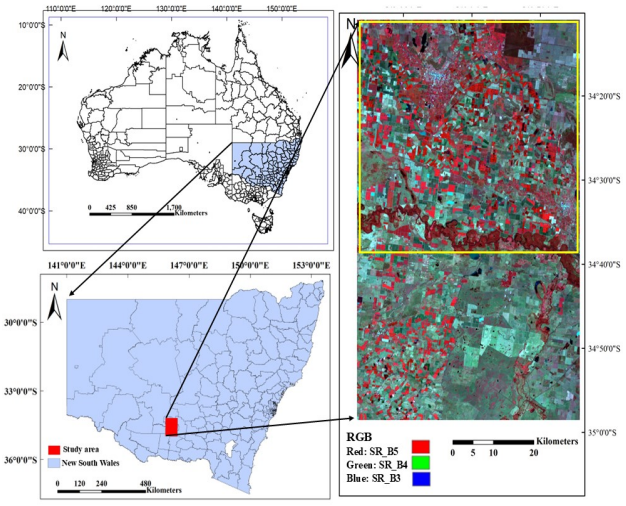

Figure 1. The study area is located in the Yanko region, New South Wales, Australia.

2.2 Data

In this study, nine pairs of LST images from the Landsat 8 and 9 sensors, along with MODIS data, were collected during the summer and autumn seasons of 2021, 2022, and 2023. The acquisition dates of the MODIS and Landsat images were identical for each image pair. In addition, the time intervals between the image pairs before and after the prediction date varied for each year, and detailed information is provided in Table 1.

2.2.1 Landsat LST data

The Landsat 8 and Landsat 9 satellites were launched on February 11, 2013, and September 27, 2021, respectively. Both satellites are equipped with Thermal Infrared (TIR) sensors that capture LST data at a spatial resolution of 100 meters. They pass over the equator at approximately 10:00 AM local time. The selected LST data are from the Level-2 Collection 2 products and were extracted using the single-channel algorithm. The Surface Temperature (ST) products from these satellites are generated based on version 1.3.0 of the Surface Temperature algorithm developed by the Rochester Institute of Technology, utilizing various datasets such as Top-of-Atmosphere (TOA) reflectance, brightness temperature, the Global Emission Database (GED), and atmospheric profiles. These data were obtained from the USGS Earth Explorer website (https://earthexplorer.usgs.gov).

2.2.2 MODIS LST data

The MOD11A1.006 product, with a spatial resolution of 1 km, is generated using the split-window algorithm based on Bands 31 and 32. The MODIS sensor, mounted on the Terra and Aqua satellites, has been providing LST data for over twenty years. The MOD11A1 product was chosen for analysis due to its temporal proximity to Landsat overpasses. The LST estimates are reported to have an accuracy of within 1.3 ˚K for homogeneous surfaces. The data was obtained from the USGS Earth Explorer website (https://earthexplorer.usgs.gov).

3. METHODOLOGY

Figure 2 presents a flowchart outlining the steps of the research process. Initially, nine pairs of satellite images acquired on different dates were subjected to geometric and radiometric corrections to ensure consistency and accuracy in the subsequent analyses. For each prediction date, two pairs of MODIS–Landsat images, along with the MODIS image of the target date, were used as inputs to the algorithms. The Landsat image corresponding to the second time point of each year served as the reference data. Using the two selected algorithms, simulated land surface temperature (LST) data were generated for the target date and subsequently compared to the reference Landsat observations. In the Random Forest (RF) algorithm, the dataset was divided into train and test sets. The model was trained using the train data, and its performance was evaluated on the test set. The ESTARFM algorithm, as a common method, was applied to the same set of input images to enable a fair comparison with the Random Forest method.

3.1 ESTARFM

ESTARFM is an advanced and improved version of the original STARFM algorithm. It was developed to enhance the accuracy of spatiotemporal fusion of satellite imagery. The algorithm requires two pairs of co-registered high-resolution and low-resolution images acquired on the same dates, and low-resolution images corresponding to the target prediction dates. A fundamental assumption of ESTARFM is that land cover changes between two reference dates follow a linear temporal trend. Based on this assumption, a linear conversion coefficient, denoted as V, is calculated for each pixel. This coefficient represents the rate of spectral change over time and serves as a critical link for transferring information between images of different spatial resolutions (Zhu et al., 2010). To enhance prediction accuracy and better utilize spatial context, ESTARFM employs a moving window approach to search for spectrally similar pixels surrounding the target pixel. The selection of these similar pixels is governed by threshold values, determined based on the standard deviation of the high-resolution image. In the next step, spectral, spatial, and temporal differences between the central pixel and the identified similar pixels are incorporated using a weighting function (Knauer et al., 2016). A weighted integration of these similar pixels then generates the final prediction for the central pixel on the target date. Ultimately, ESTARFM allows generating high-resolution predictions at any desired date within the range defined by the two base images (Guo et al., 2025).

3.2 RF

RF is a nonlinear statistical method based on the ensemble learning approach, designed for both classification and regression tasks (Breiman, 2001). It operates by constructing a collection of randomized, uncorrelated decision trees as base learners. The model then aggregates their outputs, typically through averaging for regression or majority voting for classification, to produce robust and stable predictions (Hastie et al., 2009). Two defining features of the RF algorithm are its ability to estimate out-of-bag (OOB) error and assess variable importance. During training, each tree is built using a bootstrap sample, which is drawn through random sampling with replacement from the original dataset. Consequently, approximately one-third of the observations are excluded from the training of any given tree and are referred to as out-of-bag (OOB) samples. These OOB samples are used to evaluate the model's predictive performance: each observation is predicted only by the trees for which it was not included in the training set. The average error from these predictions serves as an estimate of the model's generalization error, functioning similarly to k-fold cross-validation. Variable importance is typically assessed by measuring the improvement in the splitting criterion (e.g., reduction in residual sum of squares for regression tasks) that each variable contributes across the trees. These improvements are attributed to the respective variables at each split and are then aggregated across all trees to produce an overall importance score for each predictor (Huteng, Vohland, 2016).

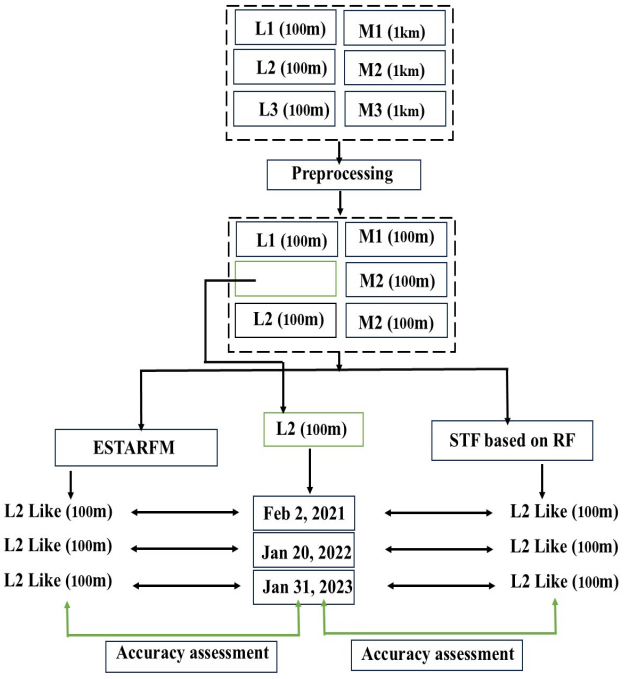

Figure 2. Workflow of the research process (L1, L2, and L3 represent Landsat LST at times 1, 2, and 3, respectively. M1, M2, and M3 represent MODIS LST at the same time steps. Time 2 is considered the simulation time for spatiotemporal fusion).

3.3 Accuracy Assessment.

In this study, the simulated LST results for January 31, 2023, January 20, 2022, and February 2, 2021, were compared with the corresponding actual Landsat observations. To evaluate the accuracy of the STF process and the degree of similarity between the simulated and observed images, three quantitative metrics were employed: Peak Signal-to-Noise Ratio (PSNR), Correlation Coefficient (CC), and Root Mean Square Error (RMSE), as defined in Equations (2) to (4) (Zhu et al., 2021; Guo et al., 2024). The RMSE metric quantifies the deviation between the predicted image and the reference image, providing a general measure of prediction accuracy. Due to its square root formulation, RMSE is more sensitive to data variability and thus offers a more precise depiction of discrepancies between the two images. Lower RMSE values indicate reduced error and

higher accuracy in the simulated image (Guo et al., 2024). The Correlation Coefficient (CC) is used to assess the degree of linear relationship between the simulated and actual images. The effective range of CC is [−1, 1], where values closer to 1 indicate greater similarity in textural details and better simulation performance (Zhu et al., 2021). Finally, PSNR serves as an indicator of image quality by measuring the ratio between the maximum possible signal and the background noise (Hore and Ziou, 2010). It is computed by first calculating the Mean Squared Error (MSE), as shown in Equation (1), and then deriving PSNR through Equation (4). Higher PSNR values suggest lower image distortion and greater resemblance between the predicted and reference images (Guo et al., 2024).

$$MSE = \frac{1}{mn}\sum_{i=0}^{m-1}\sum_{j=0}^{n-1}[y(i,j) - x(i,j)]^2 \quad (1)$$

$$RMSE = \sqrt{\frac{1}{mn}\sum_{i=0}^{m-1}\sum_{j=0}^{n-1}[y(i,j) - x(i,j)]^2} \quad (2)$$

$$CC = \frac{\sum_{i=0}^{m-1}\sum_{j=0}^{n-1}\left(x_{(i,j)}-\mu_x\right)\left(y_{(i,j)}-\mu_y\right)}{\sqrt{\sum_{i=0}^{m-1}\sum_{j=0}^{n-1}(x_{(i,j)}-\mu_x)^2(y_{(i,j)}-\mu_y)^2}} \quad (3)$$

$$PSNR = 20 \times \log_{10}\left(\frac{MAX_y}{\sqrt{MSE}}\right) \quad (4)$$

where $X(i, j)$ = actual pixel value at location (i, j)
Y (i, j) = predicted pixel value at location (i, j)
m, n = number of rows and columns in the image
MAXy maximum pixel value in the image
μx, μy = mean values of actual and predicted images

4. RESULT AND DISCUSSION

Based on Table 2, the LST simulation results highlight the significant impact of the temporal gap between base image pairs on the accuracy of spatiotemporal fusion algorithms. Specifically, the RF algorithm demonstrated minimal sensitivity to increased temporal intervals, with the RMSE rising only slightly from 1.77 ˚K to 1.81 ˚K as the interval extended from 32 to 96 days. In contrast, the ESTARFM algorithm showed a more pronounced sensitivity, with RMSE increasing from 1.69 ˚K to 2.63 ˚K over the same interval. Similarly, the SNR decreased with longer temporal gaps, from 23.20 to 21.17 ˚K for RF, and from 23.59 to 17.06 ˚K for ESTARFM. These results suggest that classical methods such as ESTARFM are more susceptible to the length of temporal intervals between base image pairs.

As shown in Figure 3, the ESTARFM algorithm performs better than the RF algorithm at shorter temporal intervals; however, its accuracy decreases as the temporal gap increases. Therefore, the use of traditional algorithms such as ESTARFM over shorter temporal intervals, and under conditions where spatial and temporal changes in land surface are limited, can lead to more accurate results and may perform better than machine learning algorithms in such cases, as observed in the results of this study. Another important aspect of this study is the temporal diversity of the input images. In addition to varying temporal intervals (32, 64, and 96 days), the acquisition dates also differ. This is an important factor that enables the assessment of algorithm resilience to both abrupt and gradual changes in cultivated lands. These changes are driven by diverse phenological variations among plant species and differences in the timing of crop growth and harvest cycles. Since the study area primarily consists of agricultural lands, the acquisition dates can influence the synchronization of the images with specific phenological stages. This synchronization or lack has a direct impact on the accuracy of spatiotemporal fusion algorithms, particularly in dynamically changing agricultural areas.

Method	Temporal Gap (Day)	RMSE (˚K)	CC	PNSR
RF	32	1.77	0.83	23.20
	48	1.70	0.82	23.78
	96	1.81	0.83	21.32
ETARFM	32	1.69	0.86	23.59
	48	2.91	0.81	19.11
	96	2.63	0.83	17.06

Table 2. LST Simulation Results.

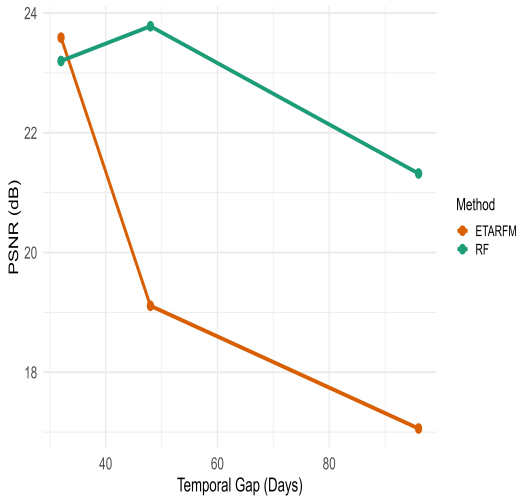

Figure 3. Simulated LST maps generated using the Random Forest and ESTARFM models over multiple temporal gaps to demonstrates the impact of varying temporal intervals between image pairs on the accuracy of simulated LST using different fusion approaches

In 2022, the base image pairs used in the spatiotemporal fusion algorithm coincided with the growth period of most crops, during which harvesting had not yet begun. This temporal alignment minimized abrupt changes in agricultural lands, thereby improving prediction accuracy, particularly for the ESTARFM algorithm. Although phenological changes are generally less pronounced over short temporal intervals, considerable phenological variability remains, not only among different species but even within the same species (Yang et al., 2024). This finding suggests that even classical algorithms can achieve higher accuracy when cloud-free images with short

temporal gaps are available. Therefore, to effectively apply spatiotemporal fusion algorithms, it is essential to select input images with appropriate temporal intervals that as closely as possible reflect the seasonal dynamics and land surface changes of the study area.

Figures 4 show the results of simulated LST using different algorithms and varying time intervals between base image pairs for different dates. The comparison between the LST simulated by the ESTARFM algorithm and the actual LST indicates that, for the dates of February 2, 2021, and January 31, 2023, the ESTARFM algorithm overestimated LST in most areas. While the Random Forest algorithm produced results more similar to the reference data.

Xie et al. (2018) also emphasized the critical role of selecting appropriate base image pairs, pointing out the accuracy of STARFM declines with longer prediction intervals due to temporal and spatial variations in land cover and phenology. This study reports that prediction accuracy was higher in forested areas than in agricultural regions (Xie et al., 2018). While some studies have proposed algorithms tailored for highly dynamic agricultural areas, their effectiveness diminishes without data from critical temporal intervals, limiting their practical applicability (Gu et al., 2023).

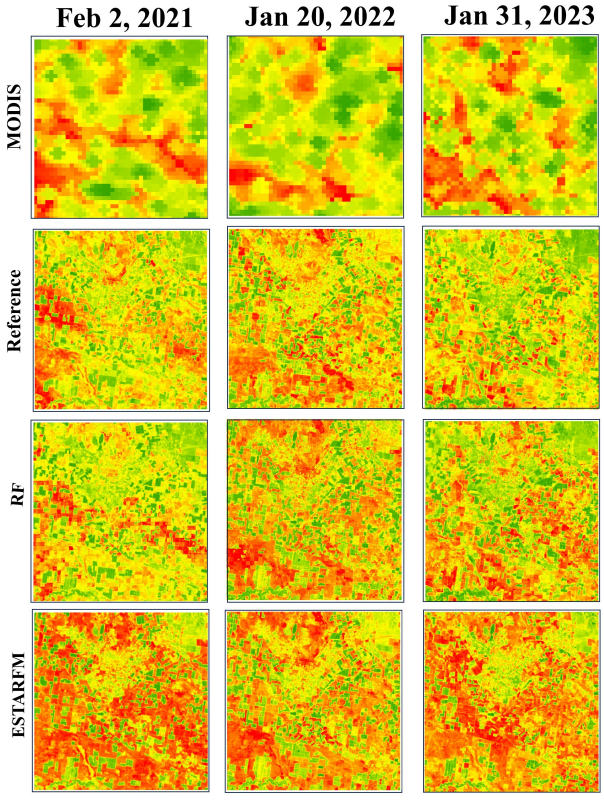

Figure 4. Simulated LST Maps for February 2, 2021, January 20, 2022, and January 31, 2023, with temporal gaps of 48, 32, and 96 days, respectively.

On the other hand, the present study reveals that at shorter temporal intervals, the performance of ESTARFM closely approaches that of the RF model, indicating that machine learning algorithms are less affected by temporal gaps and more adept at capturing phenological variations over extended periods. Previous research supports this result. For example, Filgueiras et al. (2020) demonstrated that nonlinear machine learning models outperform linear ones in generating 30-meter NDVI products using MODIS temporal resolution under significant vegetation changes. Similarly, Yang et al. (2024) compared four methods: STARFM, ESTARFM, FSDAF, and BiaSTF using various temporal intervals for simulated Landsat reflectance data. They found that intervals shorter than 40 days resulted in smoother spatiotemporal fusion and patterns more consistent with reference data. This trend was more evident in single-pair fusion algorithms, while multi-pair algorithms like BiaSTF effectively reduced the impact of temporal gaps. Among these, BiaSTF performed the best, aligning well with nonlinear growth patterns, followed by ESTARFM. These findings are consistent with the results of the current study.

5. CONCLUSION

In this study, Landsat 8 and 9 LST data were simulated for three different dates using two spatiotemporal fusion algorithms, RF and ESTARFM, under varying time intervals between base image pairs. The findings of this study indicate that the temporal gap between image pairs is a determining factor in the performance of spatiotemporal fusion algorithms. Among the evaluated methods, the classical ESTARFM algorithm showed higher sensitivity to increasing time intervals, while the machine learning-based Random Forest algorithm demonstrated more stable performance across varying temporal conditions. These differences are particularly evident in croplands, where significant phenological changes occur. Furthermore, the timing of image acquisition and its synchronization with vegetation phenological cycles play a crucial role in the accuracy of the outputs. Therefore, to ensure the effective application of spatiotemporal fusion algorithms in real-world scenarios, to achieve more accurate spatiotemporal fusion results, it is important to select base image pairs with a suitable temporal interval. Ideally, this interval should be synchronized with seasonal dynamics and surface changes in the study area to help minimize structural errors in the output. Furthermore, cloud cover is a major challenge in thermal imagery and can make challenging the implementation of spatiotemporal fusion (STF). In practice, this often necessitates selecting image pairs with longer temporal intervals, which can reduce fusion accuracy. This issue is particularly significant in temperate regions, where cloud presence may extend the temporal gap between usable images by several months.

Additionally, depending on the specific characteristics of each region, including spatial heterogeneity in land cover and the variability of vegetation cycles, there is considerable flexibility in the selection of optimal algorithms. In relatively stable environments, even classical algorithms can provide reliable and accurate results, while in areas with significant changes or longer temporal gaps between image pairs, machine learning algorithms are generally preferred. Thus, the method chosen should align with the temporal characteristics (such as seasonal or cyclic variations) and spatial features (including geographic traits and land surface properties) of the study area.

REFERENCES

Breiman, L., 2001: *Random forests, Machine learning*, 45, 5-32.

Chen, G., Lu, H., Di, D., Li, L., Emam, M., and Jing, W., 2022: StfMLP: Spatiotemporal fusion multilayer perceptron for remote-sensing images, IEEE Geoscience and Remote Sensing Letters, 20, 1-5. https: //doi.org/10.1109/LGRS.2022.3230720

Filgueiras, R., Mantovani, E .C., Fernandes-Filho, E. I., Cunha, F. F. d., Althoff, D., Dias, S. H. B., 2020: Fusion of MODIS and Landsat-Like images for daily high spatial resolution NDVI, Remote Sensing, 12, 1297. https: //doi.org/10.3390/rs12081297

Gao, F., Masek, J., Schwaller, M., Hall, F., 2006: On the blending of the Landsat and MODIS surface reflectance: Predicting daily Landsat surface reflectance, IEEE Transactions on Geoscience and Remote sensing, 44, 2207-2218. https: //doi.org/10.1109/TGRS.2006.872081

Gu, Z., Chen, J., Chen, Y., Qiu, Y., Zhu, X., Chen, X., 2023: Agri-Fuse: A novel spatiotemporal fusion method designed for agricultural scenarios with diverse phenological changes, Remote Sensing of Environment, 299, 113874. https://doi.org/10.1016/j.rse.2023.113874

Guo, H., Wang, X., Ouyang, Z., Chen, S., Che, T., Zheng, Z., 2025: Application of the ESTARFM algorithm for fusing Sentinel-2 and MODIS NDSI series in the eastern Qilian Mountains, Journal of Hydrology: Regional Studies, 57, 102103. https://doi.org/10.1016/j.ejrh.2024.102103

Guo, S., Li, M., Li, Y., Chen, J., Zhang, H. K., Sun, L., Wang, J., Wang, R., Yang, Y., 2024: The Improved U-STFM: A Deep Learning-Based Nonlinear Spatial-Temporal Fusion Model for Land Surface Temperature Downscaling, Remote Sensing, 16, 322. https://doi.org/10.3390/rs16020322

Hastie, T., Tibshirani, R., Friedman, J., 2009: The elements of statistical learning.

Hore, A., Ziou, D., 2010: Image quality metrics: PSNR vs. SSIM, 20th International Conference on Pattern Recognition, 2366-2369. //doi.org/ 10.1109/ICPR.2010.579

Huang, B., Song, H., 2012: Spatiotemporal reflectance fusion via sparse representation, IEEE Transactions on Geoscience and Remote Sensing, 50, 3707-3716.
https://doi.org/10.1109/TGRS.2012.2186638

Hutengs, C., Vohland, M., 2016: Downscaling land surface temperatures at regional scales with random forest regression, Remote Sensing of Environment, 178, 127-141.
https://doi.org/10.1016/j.rse.2016.03.006

Knauer, K., Gessner, U., Fensholt, R., Kuenzer, C., 2016: An ESTARFM fusion framework for the generation of large-scale time series in cloud-prone and heterogeneous landscapes. Remote Sens. 8, 425. https://doi.org/10.3390/rs8050425.

Moosavi, V., Talebi, A., Mokhtari, M. H., Shamsi, S. R. F., Niazi, Y., 2015: A wavelet-artificial intelligence fusion approach (WAIFA) for blending Landsat and MODIS surface temperature, Remote Sensing of Environment, 169, 243-254. https://doi.org/10.1016/j.rse.2015.08.015

Senanayake, I., Yeo, I.-Y., Walker, J., Willgoose, G., 2021: Estimating catchment scale soil moisture at a high spatial resolution: Integrating remote sensing and machine learning, Science of The Total Environment, 776, 145924. https://doi.org/10.1016/j.scitotenv.2021.145924Get rights and content

Wang, Q., Tang, Y., Ge, Y., Xie, H., Tong, X., Atkinson, P. M., 2023: A comprehensive review of spatial-temporal-spectral information reconstruction techniques, Science of Remote Sensing, 8,100102. https://doi.org/10.1016/j.srs.2023.100102

Xiao, J., Aggarwal, A. K., Duc, N. H., Arya, A., Rage, U. K., Avtar, R., 2023: A review of remote sensing image spatiotemporal fusion: Challenges, applications and recent trends, Remote Sensing Applications: Society and Environment, 32, 101005. https://doi.org/10.1016/j.rsase.2023.101005Get rights and content

Xie, D., Gao, F., Sun, L., Anderson, M., 2018: Improving spatial-temporal data fusion by choosing optimal input image pairs, Remote Sensing, 10, 1142.
https://doi.org/10.3390/rs10071142

Yang, M., Zhou, Y ,.Xie, Y., Shao, W., Luo, F., 2024: Accuracy Evaluation of Four Spatiotemporal Fusion Methods for Different Time Scales, IEEE Journal of Selected Topics in Applied Earth Observations and Remote Sensing. https://doi.org/10.1109/JSTARS.2024.3385998

Ye, N., Walker, J. P., Wu, X., De Jeu, R., Gao, Y ,.Jackson, T. J., Jonard, F., Kim, E., Merlin, O., Pauwels, V. R., 2020: The soil moisture active passive experiments: Validation of the SMAP products in Australia, IEEE Transactions on Geoscience and Remote Sensing, 59, 2922-2939.
https://doi.org/10.1109/TGRS.2020.3007371

Yee, M. S., Walker ,J. P., Monerris, A., Rüdiger, C., Jackson, T. J., 2016: On the identification of representative in situ soil moisture monitoring stations for the validation of SMAP soil moisture products in Australia, Journal of hydrology, 537, 367-381. https://doi.org/10.1016/j.jhydrol.2016.03.060

Young, R ,.Walker, J., Yeoh, N., Smith, A., Ellett, K., Merlin, O., Western, A., 2008: Soil moisture and meteorological observations from the Murrumbidgee catchment, Department of Civil and Environmental Engineering, The University of Melbourne, 610.

Zhu , X., Chen, J., Gao, F., Chen, X., Masek, J. G., 2010: An enhanced spatial and temporal adaptive reflectance fusion model for complex heterogeneous regions, Remote Sensing of Environment, 114, 2610-2623.
https://doi.org/10.1016/j.rse.2010.05.032

Zhu , X., Helmer, E. H., Gao, F., Liu, D., Chen, J., Lefsky, M. A., 2016: A flexible spatiotemporal method for fusing satellite images with different resolutions, Remote Sensing of Environment, 172, 165-177.
https://doi.org/10.1016/j.rse.2015.11.016

Zhu, X., Song ,X., Leng, P., Li, X., Gao, L., Guo, D., Cai, S., 2021: A Framework for Generating High Spatiotemporal Resolution Land Surface Temperature in Heterogeneous Areas, Remote Sensing, 13, 3885 .
https://doi.org/10.3390/rs13193885

Zhukov, B., Oertel, D., Lanzl, F., Reinhackel, G., 1999: Unmixing-based multisensor multiresolution image fusion, IEEE Transactions on Geoscience and Remote Sensing, 37, 1212-1226. https://doi.org/10.1109/36.763276

Zurita-Milla, R., Kaiser, G., Clevers, J., Schneider, W., Schaepman, M. E., 2009: Downscaling time series of MERIS full resolution data to monitor vegetation seasonal dynamics, Remote Sensing of Environment, 113, 1874-1885. https://doi.org/10.1016/j.rse.2009.04.011